OPEN ACCESS

ACTA METALLURGICA SLOVACA

2025, VOL. 31, NO. 1, 33-41

RESEARCH PAPER

The mechanical properties and microstructural changes in Inconel 718 after annealing and aging

Ayush Agarwal[1], Saurabh Dewangan[1]*

[1]Department of Mechanical Engineering, Manipal University Jaipur, Jaipur, Rajasthan, India, Pin-303007

*Corresponding author: saurabh.dewangan@jaipur.manipal.edu, tel.: 0141-3999100-838, Department of Mechanical Engineering, Manipal University Jaipur, Jaipur, Rajasthan, India, Pin-303007

Received: 20.01.2025
Accepted: 12.02.2025

ABSTRACT

A superalloy with exceptional mechanical qualities and resistance to corrosion, Inconel is heat treatable and shows microstructural alterations brought on by different heat treatment techniques. The current study focuses on the mechanical characteristics and microstructural investigation of Inconel 718 alloys that have undergone solution annealing and cooling at various media. Furthermore, the alloy plates were considered for the aging (or precipitation) process. Mechanical tests include tensile, compression, bending, and hardness tests. There were two sets of experiments: (1) taking only solution annealed & cooled samples, and (2) taking solution annealed, cooled & aged samples. To conduct each type of test, one sample was evaluated in the 'as received' condition, allowing for a proper comparison of heat treated sample properties to those of a non-treated sample. This work also includes a comparison of the characteristics of 'aged' and 'non-aged' Inconel samples. The microstructural observation demonstrated that the reduced amount of needle-shaped δ in 'unaged' samples has dramatically risen with aging. Aging resulted in thickening of the γ grain boundaries. These two microstructural modifications significantly lowered the alloy's strength and hardness. Under post-aging conditions, all heat-treated materials become highly deformable due to their reduced strength.

Keywords: Inconel 718; Solution annealing; Different cooling media; Aging; Mechanical testing; Microstructural changes

INTRODUCTION

The high-performance qualities of Inconel 718, a Ni-Cr-Nb-Mo-Fe based alloy, make it useful in nuclear power plants, aeroplane engines, turbine blades and various automobile parts [1, 2]. Because of its long fatigue life, corrosion resistivity, delayed precipitation kinetics, and sound mechanical properties at varying temperatures (from -200 to 700°C), Inconel 718 is a preferred option [3-5]. Inconel 718 possesses both γ′ and γ″ phases. The γ′ can be made predominant over γ″ if the amount of aluminium gets exceeded up to 0.5%, resulting in increased strength [6-8]. Between 600 and 750 °C is the temperature range in which γ″ forms. Orthorhombic phases develop at temperatures higher than 750 °C and dissolve at temperatures higher than 1000 °C. Carbides may be present in samples aged for a long time at temperatures between 750 and 980 degrees Celsius [9, 10]. Following the precipitation hardening process, the microstructure of Inconel 718 exhibits γ" and γ' FCC phases, which correspond to the γ matrix. There is also a secondary phase. The key component of the secondary phase is Ni3(Al, Ti) [11]. Inconel 718 has undergone thorough research due to its outstanding mechanical properties under various working environments. Some of the previous research works are discussed here:

Because of its excellent weldability, Inconel 718, a nickel-based superalloy, is perfect for laser powder bed fusion (LPBF). However, because LPBF IN718 solidifies so quickly, it has a complicated microstructure that calls for particular heat treatments. This work develops a heat treatment that optimizes material strength and improves its microstructure using FESEM, thermal mechanical analysis, and differential scanning calorimetry. For even precipitation of γ′ and γ″, the best approach is high-temperature annealing followed by two ageing processes [12]. The impact of consecutive heat treatments on Inconel 718's (I-718) ultrasonic fatigue endurance is examined in this study. Solution annealing at 1078°C for one hour, quenching in water, and double ageing at 720ºC for eight hours were all part of the heat treatment process. According to the results, heat-treated specimens exhibit a 30-fold increase in ultrasonic fatigue endurance at higher loads. Crack initiation and propagation trends were examined using Scanning Electron Microscopy analysis [13]. The study examines how the microstructure and mechanical characteristics of Inconel 718 alloy, which is produced by selective laser melting, are affected by solution and double ageing treatments. The findings indicate that when the temperature of the solution rises, more grains recrystallize, generating needle-like γ″ and nanoscale granular γ'/γ" composite phases. These characteristics are responsible for the decreased fracture elongation and increased ultimate tensile strength [14]. The “electron beam smelting (EBS)” process was used to create the Inconel 718 superalloy. The study examined how solution heat treatment affected the mechanical characteristics and precipitation behaviour. The outcomes demonstrated that EBS's quick cooling rate allows it to produce optimized microstructures. Lower temperatures cause the γ`` phase to precipitate, whereas higher temperatures cause the σ precipitates to precipitate. Coherency strengthening and antiphase boundary development were identified as the causes of the precipitation-strengthening effect, with stacking fault shearing being a major contributing factor [15]. A study looks at how the temperature of the solution treatment affects the characteristics of Inconel 718, a hot isostatically pressed superalloy. The alloy has weak ductility and poor stress rupture properties, but its strength is similar to wrought alloy in heat-treated conditions. With increasing solution temperature, the findings indicate that while strength is decreased, ductility is enhanced. Higher solution treatment temperatures may improve particle bonding and ductility, according to the study. This might produce alloy 718 components using HIP technology to its fullest extent [16]. A novel technique for creating intricate IN718 parts with little machining is metal additive manufacturing. Nevertheless, these components frequently have subpar mechanical qualities, particularly when subjected to dynamic loads. This work focuses on post-processing heat treatments to homogenize the microstructure of these additively created parts. According to the results, raising the initial heat treatment temperature decreases tensile strength while improving isotropy, Young's modulus, and ductility [17]. It was investigated how the precipitated phase in Inconel 718 alloy changed from samples that were as melted to those that were heat-treated. To attain the desired mechanical performance, a heat treatment procedure involving homogenization, solution, and aging was suggested. The treatment decreases defects brought on by grain boundary movement and expansion [18]. An intragranular δ phase was seen at 925°C, and the maximum hardness of HV 446.84 was attained at 1010°C, according to a study that examined the effects of two-step solid solution treatments on microstructure and δ phase precipitation. X-ray diffractometry analysis confirmed these findings [19]. Precipitation strengthening using Nb, Al, and Ti alloying improves Inconel 718's high-temperature performance. High strength levels are attained by alloys after extended aging, according to the cluster formula technique, which establishes alloy composition formulae [20]. The study examines the mechanical characteristics, precipitation behaviour of the γ" phase, and residual stress reduction of Inconel 718 alloy in solid solution after it has been annealed with various pretreatments. Compared to the purely aged condition, the results indicate that pretreatment decreases quenching residual stresses, encourages homogeneous nucleation and precipitation of the γ" phase, and marginally boosts yield strength [21]. A new heat treatment technique was put out to enhance the microstructure and maximise the characteristics of Inconel

718 alloy by combining twofold ageing with high-temperature ultra-short annealing at 980°C for one minute. The results shown that ultra-short annealing produced partially recrystallised nuclei and microstructure, enabling exceptional tensile characteristics and a refined microstructure [22]. Using laser-based powder bed fusion for test coupons and a "new heat-treatment condition (NHT)", the study investigates a novel heat-treatment technique for Ni-based 718 alloy. A more uniform microstructure with bigger precipitates and smaller grains is the outcome of the NHT [23]. The study looked into how hot-rolled Inconel 718 alloys' mechanical characteristics and fracture processes were affected by precipitated phases. The findings demonstrated that a double-aging treatment procedure guaranteed full precipitation and γ′ and γ″ phase expansion. Impact toughness was influenced by the precipitated δ phase's morphology, which changed from needle-shaped to granular-shaped. Intergranular cracks developed due to the needle-shaped δ phase's reduced interfacial energy compared to the granular δ phase [24]. The competition between pinning and recrystallisation of aged Inconel 718 chips is investigated in this study. The chips underwent a 10-hour age-hardening process at 600°C, which produced nanoparticle-sized precipitates that strengthened the grain boundaries. However, precipitation hardening also results from this, which reduces the material's ductility. The chips underwent post-aging heat treatment for 15 minutes at 700°C, 800°C, and 900°C to increase their ductility. The findings demonstrate that the fraction of recrystallised grains increases as temperature rises. A microstructure with the highest fraction of recrystallised grains, coincidence site lattice borders, lower grain size, and improved ductility is produced at 900°C [25]. The necessity for stability in harsh settings has raised demand for high-strength materials, especially Inconel 718. Precipitation stages, impacted by ageing circumstances, affect the alloy's strength. The highest strength and hardness were noted following heat treatment at 718°C because of increased precipitation size and quantity, according to this study's investigation into the relationship between precipitation behaviour and mechanical parameters [26]. The study looks at the cutting mechanisms of Inconel 718 alloy under different grain refinement patterns and heat treatment procedures. Cutting force, cutting temperature, and surface grain refinement are all examined concerning heat treatment procedures and cutting parameters using a constitutive model and DEFORM-3D simulation. The findings indicate that cutting force increases most when the alloy is aged from 668°C to 718°C, and that cutting speed has a negative relationship with this rise. According to the study, the workpiece's grain size reduces during the cutting process and increases with cutting depth [27]. The work emphasises the significance of post-AM double ageing heat treatment (HT) for laser-based powder bed fusion (L-PBF)-fabricated alloy IN718. Microhardness, microstructural alterations, and flaws caused by AM were all successfully closed by the HT method. The HT microstructure has a homogeneous austenite gamma matrix with heterogeneous columnar dendrites and laves phases. Grain boundary development and dislocation were stopped by the δ phase, exposing finer grain structures. Following HT, micro-computed tomography (micro CT) analysis showed no AM-induced porosity. The heat-treated samples' hardness rose from 417 to 564 HV to 35%. Thermal loading caused a volumetric shrinkage of 3.084%, according to dimensional analysis [28]. A study examined the impact of solution-annealed treatment on the microstructure and chemical properties of Inconel 718 superalloys, revealing that epitaxy and thermal dissipation led to massive columnar austenite grains. At the same time, the SA sample prevented advantageous hardening phases [29]. Several annealing processes were applied to the Inconel 718 alloy, which was made by selective laser melting. With flat grain boundaries and numerous annealing twins, the microstructure is recrystallised. After annealing, the microhardness, tensile strength, and yield strength all rise, while elongation falls following fracture. After a solution dual ageing annealing and double ageing annealing, the fatigue properties marginally improve, while uniform double ageing annealing results in a minor decline [30]. With an emphasis on tensile and creep characteristics, this study investigates the direct ageing effect on Inconel 718 forged components. The findings demonstrate that direct ageing improves DA specimens' tensile and creep characteristics. However, the effect is caused by a lower δ phase content rather than a larger residual strain hardening level in the microstructure. The study discovered that while residual forging strain hardening had no discernible impact on tensile and creep capabilities, an increase in δ phase composition degrades mechanical performance [31].

The present work is an extension of work done in [32]. In the previous version, the Inconel 718 alloys were solution annealed and then cooled in different media such as sand, water, and furnace. This way, the cooled samples were tested for altering mechanical properties and microstructure. The present work applies a common ageing process to all the solution-annealed & quenched samples. The properties of 'non-aged' and 'aged' samples have been compared in this work. Hence, the applicability of ageing (or precipitation) has been discussed in light of the mechanical properties of Inconel 718 alloy.

MATERIALS AND METHODOLOGY

As the current work is an extension of the work done in [32], initial experimental works are the same as discussed in previous work. Four Inconel-718 alloys with dimensions 100×50×12 mm were taken for the heat treatment. All the plates were collected in a cold rolled state. The EDS analysis has been done to check the constituent elements in the Inconel 718 alloy considered under study **Fig. 1**. Also, the XRD analysis has been carried out to check various compounds and phases in the alloy (**Fig. 2**). The amount (weight %) of Ni, Cr, Mo, and Fe are 39.6%, 16.6%, 6%, and 14.6% respectively. The availability of *C* and *O* can be an indication of adhering organic particles during the handling of the sample. *K*, *Ti*, *Mn*, and *Zn* may be neglected as their error is quite high.

The traditional heat treatment of Inconel alloys involves solution annealing in the range of 925°-1010°C for a few hours, followed by rapid cooling, preferably in chilled water. Then, it is precipitated by incorporating secondary phases like γ′ and γ″, induced at 600-800°C, with aging elements like Al, Ti, and Nb in solution [33, 34].

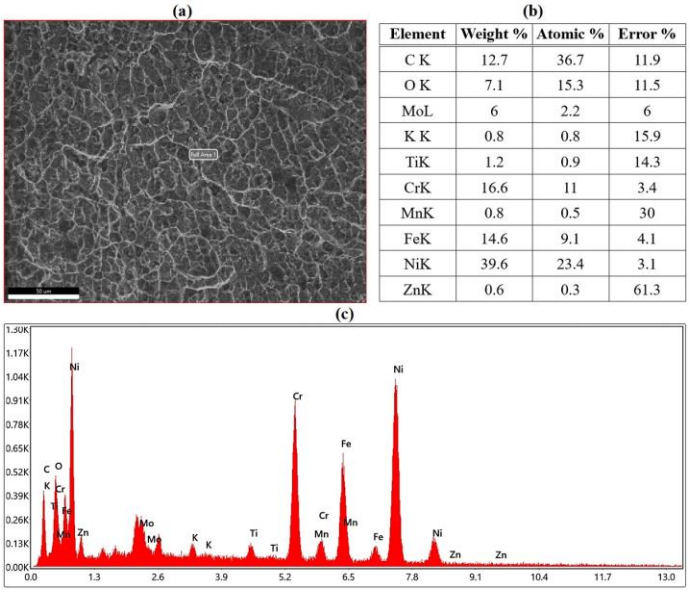

Element	Weight %	Atomic %	Error %
C K	12.7	36.7	11.9
O K	7.1	15.3	11.5
MoL	6	2.2	6
K K	0.8	0.8	15.9
TiK	1.2	0.9	14.3
CrK	16.6	11	3.4
MnK	0.8	0.5	30
FeK	14.6	9.1	4.1
NiK	39.6	23.4	3.1
ZnK	0.6	0.3	61.3

Fig. 1 EDS analysis into Inconel 718 plate used under study

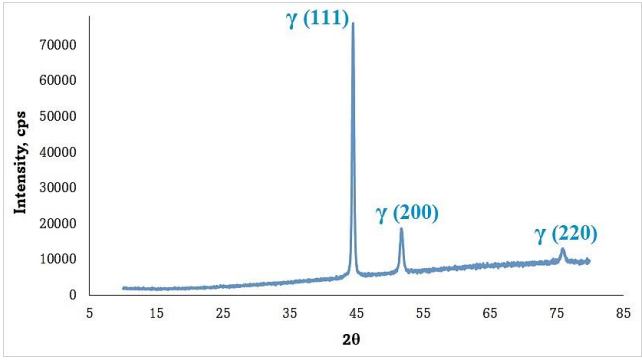

Fig. 2 XRD analysis of Inconel 718 plate

In the previous work [32], only solution annealing and cooling were done during the heat treatment of the Inconel 718 samples. The first was kept in 'as received' condition while 2nd the 3rd and 4th plates underwent solution annealing in which they were heated at a constant temperature of 900°C for 2 hr of duration. After this heating period, samples were taken from the furnace and cooled in different

media. The 2nd plate was buried in the sand so no part of the plate could be exposed to the atmosphere. The 4th plate was quenched in water, while the 3rd one was left inside the closed chamber induction furnace. After collecting all the annealed & cooled plates, reheating was done again. The reheating was done at 700°C for 4 hours in a closed chamber induction furnace. After 4 hours, the furnace was switched off, and the samples were only allowed to cool in the closed furnace. These samples took nearly. This reheating was done to dissolve the ageing elements in the metal solution. The complete experimental procedure is shown in **Fig. 3**. The practical conditions adopted in each sample are written in **Table 1**.

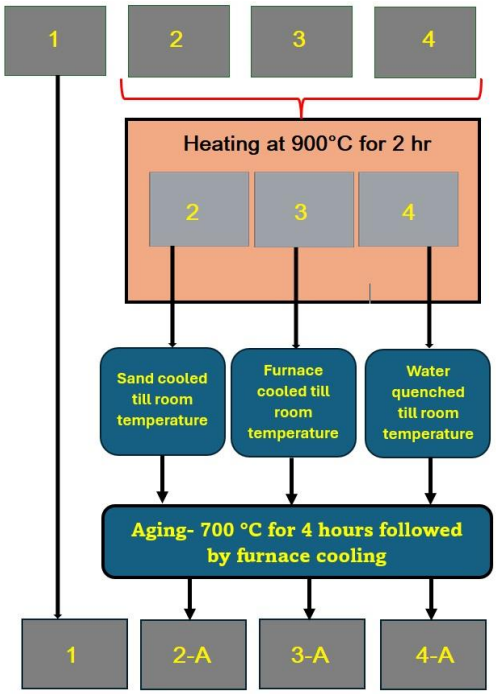

Fig. 3 Experimental procedure in this work

After heat treatment, four destructive mechanical tests, such as tensile, compression, three-point bending, and hardness tests, were conducted on the samples. These properties of aged samples have been compared with those of only annealed & cooled samples. The standard norms have been followed as suggested by the ASTM to prepare the specimens for the tests. The tensile specimens were cut according to ASTM-E8 standard. The grip and gauge lengths were 30 mm and 25 mm for each specimen. For compression test, the cube shaped specimen of dimension 12×12×12 mm^3 was cut as per the standard suggested by ASTM-E9. Similarly, ASTM E290 standard was followed for the specimen of bending test. Rockwell-C scale hardness test was conducted on the remaining part of the four plates. The tensile, compressive and bending tests were performed on a 'universal testing machine (UTM)' with a maximum load capacity of 400 kN. The strain rate of 0.1 s^{-1} was selected for tensile and compression test while the deformation rate for bending test was 10 mm/min. The small pieces of all the four plates were machined-off to make them specimens for microstructural analysis. For this purpose, an optical microscope was utilized to capture photographs at 200X and 500X magnifications. Before that, a thorough polishing and etching procedure was done. Multiple grades of abrasive papers were utilized to polish the samples. Kalling's reagent was taken as etchant in this study. The samples were dipped into the solution for 5-8 seconds and then wiped off with cotton before microstructure observation.

RESULTS ANALYSIS

Tensile test: The tensile test results were plotted under stress-strain diagram. For specimen 1, there is only one curve while a comparative stress-strain curves have been plotted for 2nd, 3rd and 4th. A comparative tensile property between only solution annealed and solution annealed+aged samples is discussed in **Table 2**. All the stress-strain curves are shown in **Fig. 4**.

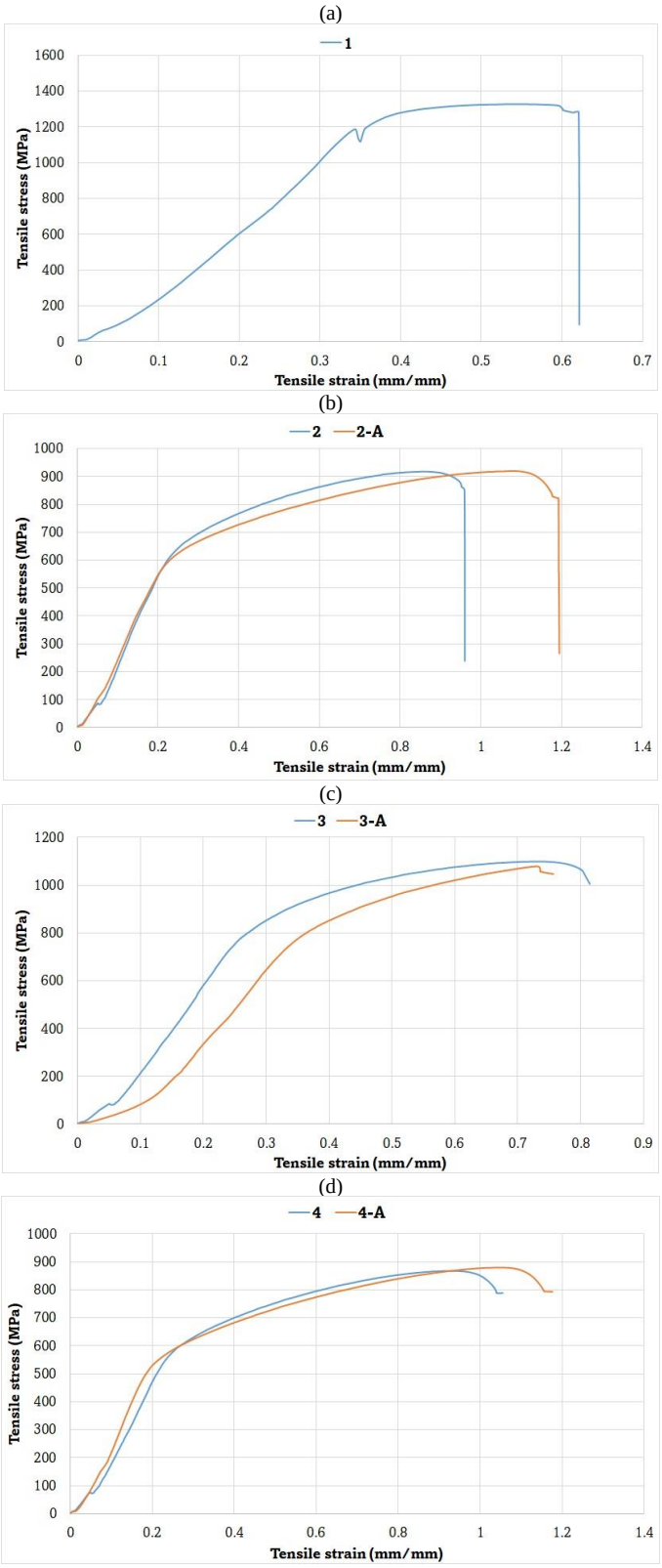

Fig. 4 Tensile test results as stress-strain diagram

Table 1 Physical conditions and sample naming according to the experimental work performed on the Inconel plates

Sr. No.	Stage 1: solution annealing + cooling	Sample naming	Expected Cooling rate after stage-1	Stage 2: Aging	Expected Cooling rate after stage-2	Sample naming
1.	As received (Not heat treated)	**1**	--	--	--	**1**
2.	Annealed at 900°C for 2 hr of soaking time followed by cooling in *sand* until room temperature	**2**	0.048 °C/s	Reheated in furnace at 700°C for 4 hr and cooled in the same furnace	0.006 °C/s	**2-A**
3.	Annealed at 900°C for 2 hr of soaking time followed by cooling in *furnace* until room temperature	**3**	0.008 °C/s	Reheated in furnace at 700°C for 4 hr and cooled in the same furnace	0.006 °C/s	**3-A**
4.	Annealed at 900°C for 2 hr of soaking time followed by quenching in *water* until room temperature	**4**	14.467 °C/s	Reheated in furnace at 700°C for 4 hr and cooled in the same furnace	0.006 °C/s	**4-A**

Table 2 Tensile test results at 'solution annealed state' and at 'aging' condition (1* = this sample was not heat treated)

Sample	Ultimate tensile strength (MPa)		Max. Disp. (mm)		Yield stress (MPa)		Elongation (%)		UTS to YS ratio	
	At solution annealed state	After aging	At solution annealed state	After aging	At solution annealed state	After aging	At solution annealed state	After aging	At solution annealed state	After aging
1*	1329		15.54		1188		20.88		1.118	
2	917	919.474	24.0	29.87	640	563.558	44	55.20	1.433	1.632
3	1099	1078.834	20.4	18.92	807	798.890	34	20.40	1.362	1.350
4	868	879.428	26.4	29.41	573	503.985	46	53.48	1.515	1.745

Specimen 1, being in the 'as received' cold rolled condition, has shown the highest value of UTS of 1329 MPa, reached after a maximum load application of 98 kN. The yielding occurred after crossing the YS of 1188 MPa. A total elongation of 15.5 mm was recorded till the fracture of the specimen 1 with overall elongation of 20.88%. The UTS to YS ratio for this specimen is 1.118. This low value reveals no huge gap between the stresses at yield point and UTS point. Specimen 2, at solution annealed and sand cooled state, has reached UTS of 917 MPa which is quite lower than 'as received' sample. The UTS and YS of specimen 2 are 29% and 45%, respectively, less than those of specimen 1. The UTS to YS ratio for specimen 2 is 1.433. The significant reduction in the YS of sample 2 shows an early beginning of yielding, and hence, the elongation is also significantly enhanced after sand cooling. After the ageing process, specimen 2-A has shown a further drop in YS (563 MPa), nearly 12% less than the 'unaged' sample. The UTS of specimen 2-A is almost the same, but the elongation of specimen 2-A has increased to 30 mm. Also, the UTS to YS ratio for specimen 2-A, i.e., 1.632, is higher than for specimen 2. Hence, cooling sand and aging have considerably reduced the strength of the sand, with an increase in ductility. The specimen 3, the furnace cooled, has 1099 MPa of UTS which is higher than specimen 2. The YS and elongation are 807 MPa and 20.4 mm respectively. It is shown 34% elongation till fracture. But, after aging, means specimen 3-A has shown a minor drop in every parameter as compared to 'unaged' condition. Hence, compared to specimen 3, specimen 3-A showed 2% less UTS, 1% reduced YS, and nearly similar total elongation (19 mm). Considering **Fig. 4(c)**, it can be seen that less load is required to reach up to yield point and UTS point in 3-A specimen. Also, the area under the stress-strain curve for specimen 3-A is lesser than the 'unaged' specimen. So, aging has reduced the strength of the specimen 3. However, the ratio of UTS and YS for specimen 3 and 3-A is almost same (≈1.35). Specimen 4, being solution annealed & water quenched, possessed very low value of UTS (868 MPa) and YS (573 MPa) among all 'unaged' specimens. Upon aging, specimen 4-A has further lost its YS by 12% although some parameters like UTS, and elongation are increased by 12% and 11.4% respectively. Also, the total % elongation is increased after aging. In **Fig. 4(d)**, it can be observed that yield point can be achieved early in the aged sample. The plastic zone to the UTS point has increased compared to the 'unaged' sample. This means that better strain hardening occurs after the ageing process. The high UTS has seen it to YS ratio value, i.e., 1.745. The overall ductility shows a significant improvement after water quenching and aging.

Further, the fractured surface of the broken tensile specimens was analyzed by FESEM images (**Fig. 5**). By considering same magnification (1000 X) and scale (10 μm), all the pictures were captured and compared with each other. Specimen 1 has shown numerous dimples on the fractured regions which leads to high degree of plastic deformation and dimple fractures. Dimples are the indications of ductile failure [42, 43]. Apart from dimple fracture, the specimen 2-A has shown some facets caused by intergranular fracture [43] and a layered δ phase throughout the fractured zone. The specimen 3-A was noticed with macro-dimples along with micro-dimples. Similar to specimen 2-A, the lamella of δ phase was seen over the fractured grains. Again, the similar attributes of plastic deformation and δ phase were observed in specimen 4-A.

(a)

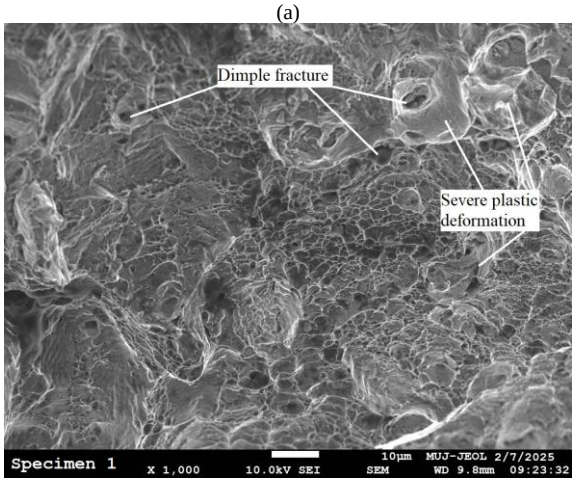

(b)

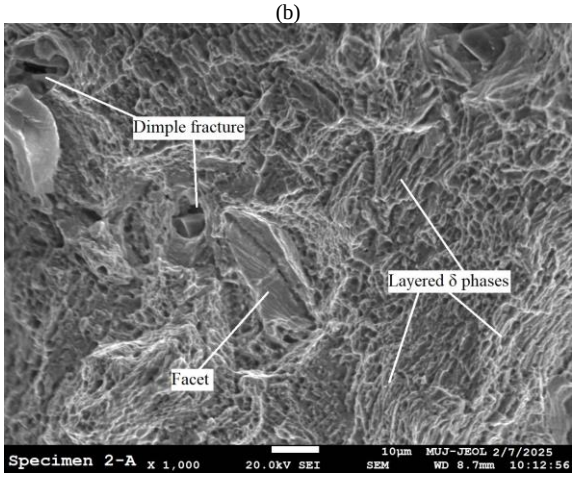

(c)

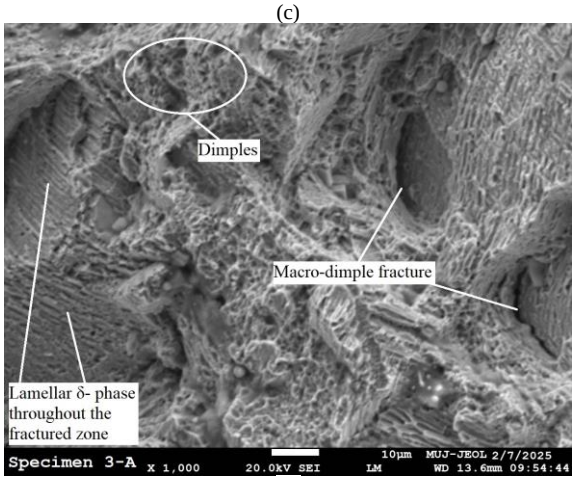

(d)

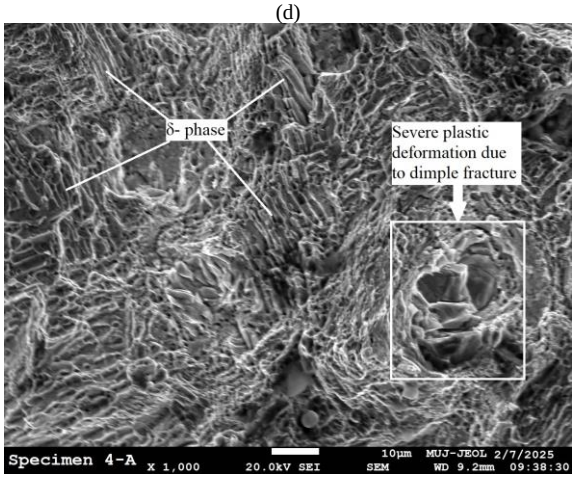

Fig. 5 Fractography analysis of fractured surface of tensile specimens: (a) Specimen 1; (b) Specimen 2-A; (c) Specimen 3-A; (d) Specimen 4-A

Bending test: The *three-point bending* test was performed on all the specimens so that a common deformation value, i.e., 45 mm, can be achieved during loading. The curves obtained between load and displacement after the bending test are shown in **Fig. 6**. Specimen 1 applied a maximum load of 4 kN to cross its ultimate point from where a drop in load application begins. Specimen 2 has greatly improved the load requirement for achieving the ultimate point. The maximum load required for specimen 2 is 9.4 kN. This load requirement has significantly reduced after performing aging in specimen 2. The load of 1.2 kN was sufficient to reach up to the ultimate point in specimen 2-A. Similarly, the maximum load values for specimen 3-A (2.8 kN) and 4-A (1.6 kN) are considerably reduced after aging phenomenon. The reduced load requirement indicates that the bending modulus of the aged specimen has been reduced, and hence, they can be deformed easily. In other words, the aging has improved the ductile nature of all the aged specimens.

(a)

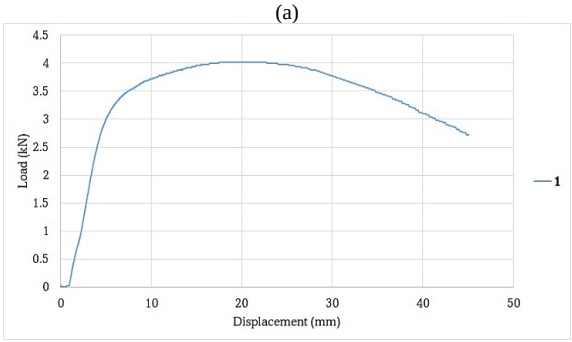

(b)

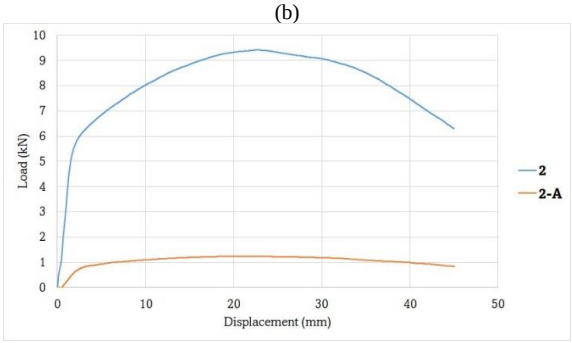

(c)

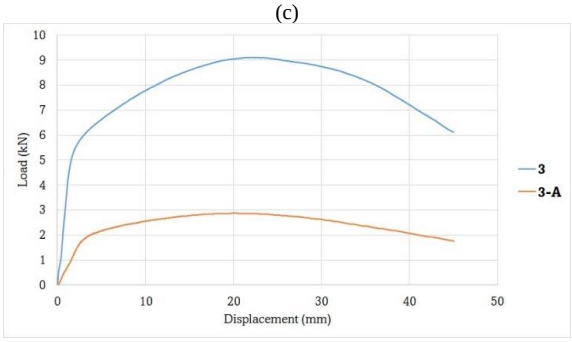

(d)

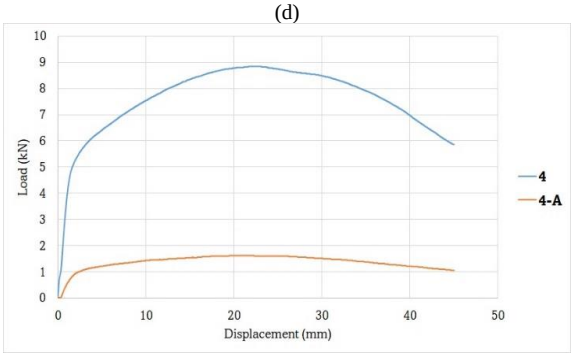

Fig. 6 Load vs displacement curves obtained by three point bending test

Compression test: Like the bending test, the compression test has been performed until the specimens reach a certain final height. The initial height of all the cube-shaped specimens was 12 mm, which finally was reduced by 5.5 mm. Means, the final height of the specimens becomes 6.5 mm. The load requirement for compression of 5.5 mm is assessed for each specimen. The load-displacement curves obtained by the compression test are shown in **Fig. 7**. For the as-received

specimen -1, the load requirement is 340 kN. It is the maximum amount of load among all the specimens because the as received sample is in cold-rolled state. After solution annealing all the specimen got more ductile and hence less amount of load was required to deform till a certain height. Specimens 2, 3 and 4 are applied 238 kN, 325 kN, and 288 kN of loads for the deformation. Specimen 2-A has shown 330 kN load value for 5.5 mm of deformation. Other two specimens have lost their strength after the aging process because the load values have further decreased in post-aged conditions. Specimens 3-A and 4-A got deformed, till 6.5 mm of final height, at the load values of 310 kN and 280 kN respectively. In this condition, again, 'solution annealed, water quenched & aged' specimen has shown the highest ductility among all.

(a)

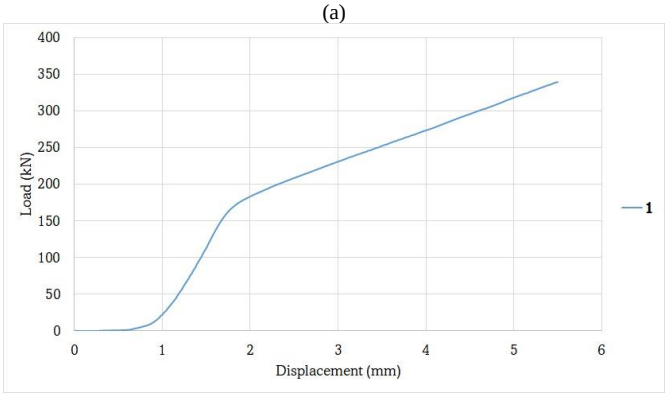

(b)

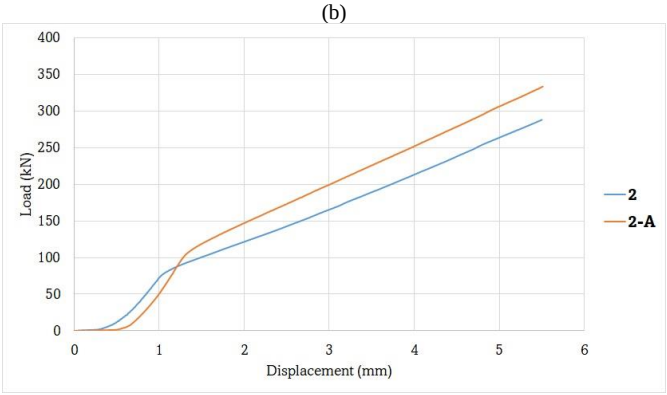

(c)

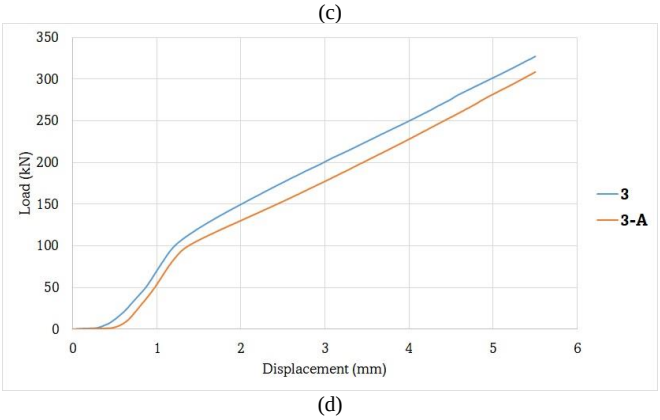

(d)

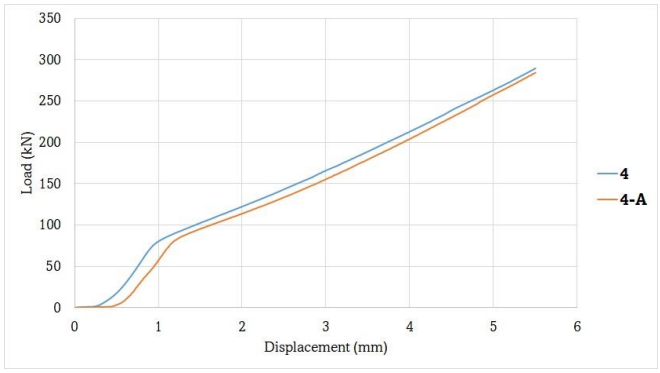

Fig. 7 Load-displacement curves obtained by compression test

Hardness test: The hardness of various samples is shown in a comparative bar chart (**Fig. 8**). The hardness of 1st specimen is 26 HRC. Also, this is the highest hardness recorded among all the samples. In sample 2, after sand cooling, the hardness gets reduced, but it has increased after following aging on the sand cooled sample. The hardness of samples 3-A and 4-A have been negatively affected after undergoing aging processes. The results of hardness test are in good corroboration with those of compression test.

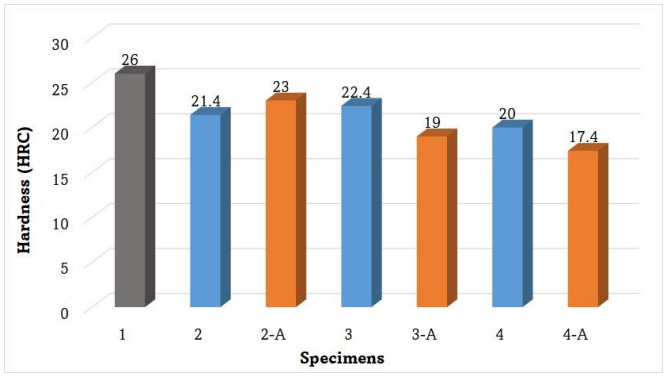

Fig. 8 Hardness results in different samples under study

Microstructural observation: The optical micrography has been done to check the grains' structure and phases in all the samples (**Fig. 9**). The microstructure of specimen 1, as received specimen, carries bright grains of γ austenite with many twins [35, 36] over there. The γ is stable due to Ni, Cr, and Mo presence in Fe. Fine metal carbides can be recognized by their tiny black appearance. These carbides are evenly distributed in the γ grains. This even distribution of carbides ensures the high strength and hardness of the alloy, which has also been proved in the current study. The as received sample has shown the highest strength and hardness. The specimen 2 has shown some visible changes at the microstructural level. Two additional appearances of δ phase and carbonitrides have been noted. The δ phase is mainly precipitated as needle shape over the austenite grains whereas the carbonitrides (Ti-rich) are the globular shaped structure with peach in colour [37]. The metal carbides ($M_{23}C_6$) [38-41] are also visible in this specimen. After following the aging process, the specimen 2-A has shown a substantial change in the appearance. The needle- shaped δ phase has excessively increased over the γ grains, yet the carbonitrides are unchanged. Due to increased δ phase, the UTS and YS have been negatively affected after aging. The specimen 3, a furnace cooled sample, has shown a similar appearance as sample 2. A multiple twins, carbonitrides and some δ are visible. However, once specimen 3 was aged, these appearances suddenly altered. The δ phase has been greatly enhanced throughout the γ matrix by solution annealing, furnace cooling followed by aging. Also, the prolonged heating has enhanced the thickness of γ grain boundary due to displacement of alloying elements towards the boundary. The excessive δ and thick grain boundary are the reasons behind reducing the tensile strength and increasing the deformation rate in specimen 3-A. The specimen 4 has also shown a similar attribute of microstructure as sample 3. Like other aged specimens, specimen 4-A has also shown excessive growth of δ phase on the austenite grains. The grain boundary thickening is also prominent in specimen 4-A.

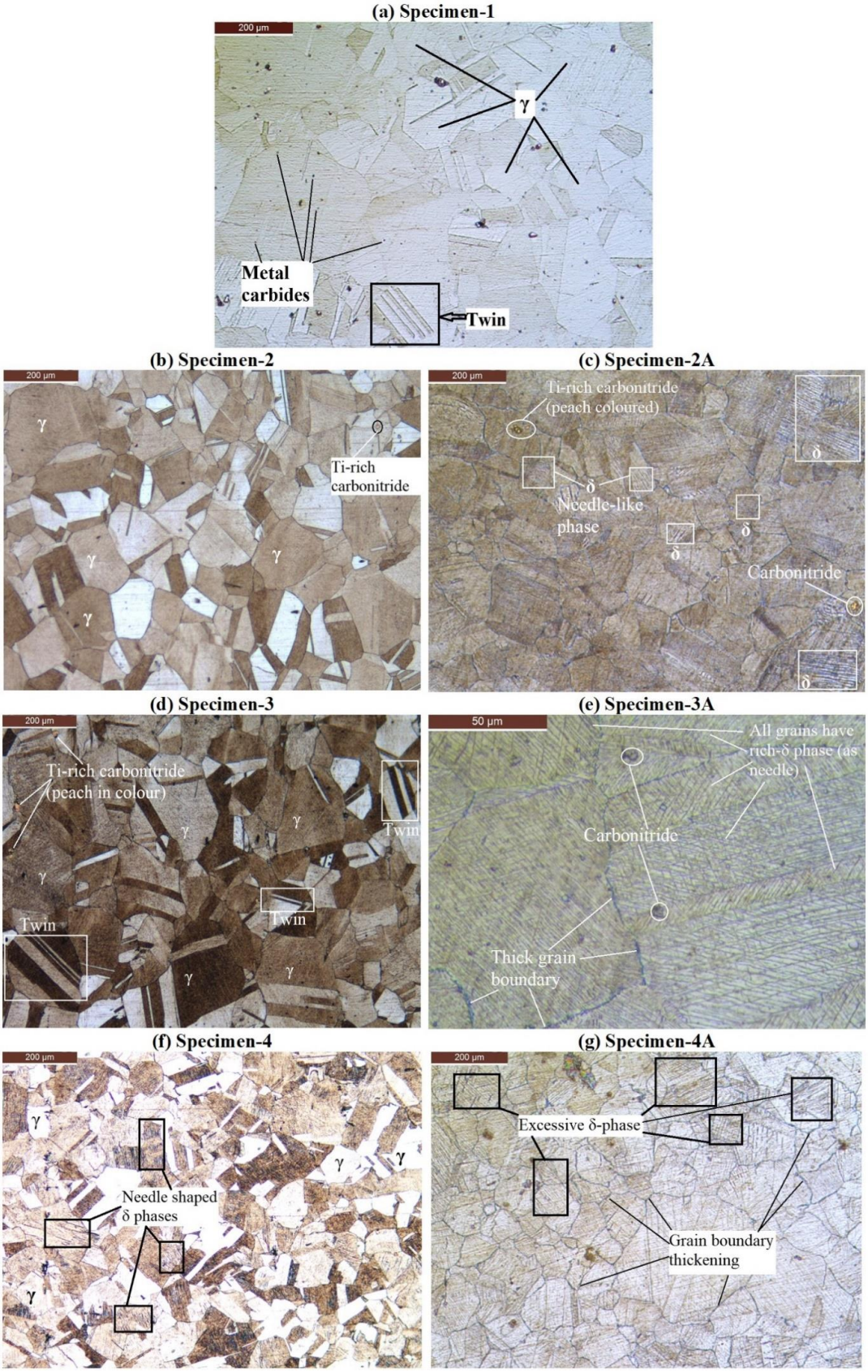

Fig. 9 Microstructural analysis: (a) Specimen 1; (b) Specimen 2; (c) Specimen 2-A; (d) Specimen 3; (e) Specimen 3-A; (f) Specimen 4; (g) Specimen 4-A

CONCLUSION

Inconel 718 is utilized in a wide range of high temperature applications, such as aircraft fasteners, turbine blades, and jet engines. As a result, its properties need to be examined after a lengthy period of high temperature heating. In this work, an attempt has been made towards the mechanical properties and microstructural analysis of Inconel 718 alloys following solution annealing and cooling, as well as the aging process. It compares the properties of heat-treated and untreated samples, focusing on the aging process and distinguishing the characteristics of 'aged' and 'non-aged' Inconel samples. The following conclusions can be made based on outcomes of this work:

- The as received specimen's microstructure comprises of fairly bright γ austenite grains with numerous twins, ensuring good strength and hardness. Upon solution annealing & cooling, a noticeable modification, including the insertion of δ phase and carbonitrides has been noticed. After aging, the needle-shaped δ phase has risen over the γ grains. In addition, with increment of δ phase, γ grain boundary thickening has also been noticed. The aging process has harmed the UTS, YS, bending strength and compressive strength, although the ductility has increased drastically in the aged samples.
- According to the tensile test results, the 'as received specimen' has shown the maximum UTS (1329 MPa) and YS (1188 MPa) among all the samples. The maximum elongation of this samples was 15.5 mm. Specimen 2, the sand cooled, has a 29% and 45% lower UTS and YS, respectively, than these specimen 1. After aging, a further decrement of 12% in YS was recorded as compared to solution annealed & sand cooled sample. Similarly, specimen 3 also showed a minor drop in all the tensile parameters. It requires less load to reach the yield and UTS points and has a lesser stress-strain curve area than an 'unaged' sample. Specimen 4, solution annealed & water quenched, had low UTS and YS values among unaged specimens. Aging reduced YS by 12%, but increased UTS and elongation by 12% and 11.4%, respectively. The aged sample achieved a yield point early, indicating better strain hardening.
- The bending test result establishes that the aged samples require less load to get deformed. In other words, aging has decreased the bending modulus of Inconel 718 alloy.
- During compression, only the received sample took the maximum load to get compressed to a certain height. After solution annealing, the specimens became more ductile and required less force to distort. This load requirement has again decreased for the aged samples.
- The aging process has reduced the hardness of the samples. The water quenched and aged sample shows the lowest hardness value.

In the future, the high-temperature tensile, fatigue, and creep tests can be followed for a detailed mechanical property analysis after heat treatment. Also, the phase fraction analysis may provide an exact quantification of phases after performing the heat treatment on Inconel 718 alloy.

References

[1] E. Chlebus, K. Gruber, B. Kuźnicka, J. Kurzac, T. Kurzynowski: Materials Science and Engineering: A, 639, 2015, 647-655. https://doi.org/10.1016/j.msea.2015.05.035

[2] S. Dewangan, S. Narayanan, G.S. Gill, U. Chadha: Acta Metallurgica Slovaca, 29(1), 2023, 5-9. https://doi.org/10.36547/ams.29.1.1664

[3] D.E. Mongeau, W. Wallace: Scripta Metallurgica, 9(11), 1975, 1185-1188. https://doi.org/10.1016/0036-9748(75)90405-6

[4] V.G. Krishna, G.D. Janakiram, C.H.V.S. Murty, M. Srinivas, A.V. Reddy: Practical Metallography, 45(10), 2008, 495-504. https://link.springer.com/article/10.1007/s40032-024-01158-5

[5] A. Agarwal, A. Modi, N. Sharma, S. Dewangan: Acta Metallurgica Slovaca, 30(4), 2024, 171–177. https://doi.org/10.36547/ams.30.4.2093

[6] D. Raynor, J.M. Silcock: Metal Science Journal, 4(1), 1970, 121-130. https://doi.org/10.1179/msc.1970.4.1.121

[7] C.T. Sims, N.S. Stoloff, W.C. Hagel (eds.): *Superalloys II* (Vol. 8), New York: Wiley, 1987.

[8] M. Zouari, N. Bozzolo, R.E. Loge: Materials Science and Engineering: A, 655, 2016, 408-424. https://doi.org/10.1016/j.msea.2015.12.102

[9] M.D. Mathew, P. Parameswaran, K.B.S. Rao: Materials Characterization, 59(5), 2008, 508-513. https://doi.org/10.1016/j.matchar.2007.03.007

[10] A. Sukumaran, R.K. Gupta, V. Anil Kumar: Journal of Materials Engineering and Performance, 26, 2017, 3048-3057. https://doi.org/10.1007/s11665-017-2774-8

[11] W.M. Tucho, P. Cuvillier, A. Sjolyst-Kverneland, V. Hansen: Materials Science and Engineering: A, 689, 2017, 220-232. https://doi.org/10.1016/j.msea.2017.02.062

[12] E. Bassini, G. Marchese, A. Aversa: Metals, 11(6), 2021, 921. https://doi.org/10.3390/met11060921

[13] G.M.D. Almaraz, M.G. Tapia, I.F.Z. Tello: Procedia Structural Integrity, 39, 2022, 281-289. https://doi.org/10.1016/j.prostr.2022.03.098

[14] P. Bai, et al.: Journal of Alloys and Compounds, 911, 2022, 164988. https://doi.org/10.1016/j.jallcom.2022.164988

[15] X. You, et al.: Materials Science and Engineering: A, 689, 2017, 257-268. https://doi.org/10.1016/j.msea.2017.01.093

[16] G.A. Rao, M. Srinivas, D.S. Sarma: Materials Science and Technology, 20(9), 2004, 1161-1170. https://doi.org/10.1179/026708304225022124

[17] A.A. Alafaghani, M.A. Ablat, H. Abedi, A. Al Gamal, A. Qattawi: JOM, 74(12), 2022, 4772-4786. https://doi.org/10.1007/s11837-022-05498-4

[18] W. Wang, Z. Chen, W. Lu, F. Meng, T. Zhao: Journal of Alloys and Compounds, 913, 2022, 165171. https://doi.org/10.1016/j.jallcom.2022.165171

[19] E. Liu, et al.: International Journal of Minerals, Metallurgy and Materials, 31(10), 2024, 2199-2207. https://doi.org/10.1007/s12613-024-2887-7

[20] Y. Li, et al.: Materials Science and Engineering: A, 2024, 146803. https://doi.org/10.1016/j.msea.2024.146803

[21] J. Zhu, W. Yuan: Journal of Alloys and Compounds, 939, 2023, 168707. https://doi.org/10.1016/j.jallcom.2023.168707

[22] R. Ran, et al.: Transactions of Nonferrous Metals Society of China, 34(7), 2024, 2204-2218. https://doi.org/10.1016/S1003-6326(24)66535-0

[23] S. Choudhary, V. Gaur: Materials Science and Engineering: A, 911, 2024, 146930. https://doi.org/10.1016/j.msea.2022.144484

[24] Y. Zhang, L. Lan, Y. Zhao: Materials Science and Engineering: A, 864, 2023, 144598. https://doi.org/10.1016/j.msea.2023.144598

[25] P.C. Yadav, S. Shekhar, B. Jayabalan, N.K. Sharma: Materials Chemistry and Physics, 295, 2023, 127098. https://doi.org/10.1016/j.matchemphys.2022.127098

[26] G.H. Lee, et al.: Journal of Materials Research and Technology, 27, 2023, 4157-4168. https://doi.org/10.1016/j.jmrt.2023.10.196

[27] P. Zhang, et al.: Vacuum, 227, 2024, 113442. https://doi.org/10.1016/j.vacuum.2024.113442

[28] V.P. Kumar, A.V. Jebaraj: Transactions of the Indian Institute of Metals, 74(12), 2021, 3103-3117. https://doi.org/10.1007/s12666-021-02374-8

[29] G.K. Sujan, H. Li, Z. Pan, D. Liang, N. Alam: Additive Manufacturing, 51, 2022, 102602. https://doi.org/10.1016/j.addma.2022.102602

[30] L. Li, X. Zhu, F. Tian, Y. Chen, Q. Liu: Matéria (Rio de Janeiro), 27, 2022, e20220214. https://doi.org/10.1590/1517-7076-RMAT-2022-0214

[31] A. Nicolaÿ, J.M. Franchet, N. Bozzolo, J. Cormier: Metallurgical analysis of direct aging effect on tensile and creep properties in inconel 718 forgings. In *Superalloys 2020: Proceedings of the 14th International Symposium on Superalloys*, Heidelberg: Springer International Publishing, 2020, pp. 559-569. https://doi.org/10.1007/978-3-030-51834-9_54

[32] P. Agarwal, S. Jha, S. Dewangan, A. Agarwal: Journal of Materials Engineering and Performance, 2024, 1-16. https://doi.org/10.1007/s11665-024-10520-8

[33] Special Metals: https://www.specialmetals.com/documents/technical-bulletins/inconel/inconel-alloy-718.pdf (Date of access: 18-Aug-2024).

[34] Inconel 718 (TECH STEEL & MATERIALS): https://www.techsteel.net/alloy/inconel-718#:~:text=Overall%2C%20three%20heat%20treatments%20are,F%20(620%C2%B0C). (Date of access: 18-Aug-2024).

[35] Metals and Alloys: https://www.phase-trans.msm.cam.ac.uk/abstracts/annealing.twin.html#note (Date of access: 22-May-2024).

[36] S. Dewangan, G. Maheshwari, Shajar, A. Agarwal, V. Prakash: Journal of The Institution of Engineers (India): Series C, 2024, 1-12. https://doi.org/10.1007/s40032-024-01158-5

[37] Carpenter Technology: https://www.carpentertechnology.com/blog/nickel-base-superalloy-718-microstructure-characterization (Date of access: 22-May-2024).

[38] S. Heo, Y. Lim, N. Kwak, C. Jeon, M. Choi, I. Jo: Metals, 14(4), 2024, 440. https://doi.org/10.3390/met14040440

[39] A. Modi, N. Sharma, O. Sharma, S. Dewangan, R. Varshney: Journal of The Institution of Engineers (India): Series D, 2024, 1-11. https://doi.org/10.1007/s40033-024-00668-x
[40] A. Agarwal, G. Maheshwari, Shajar, S. Dewangan: Canadian Metallurgical Quarterly, 2024, 1-12. https://doi.org/10.1080/00084433.2024.2429182
[41] H. Guan, W. Jiang, J. Lu, Y. Zhang, Z. Zhang: Materials Today Communications, 36, 2023, 106582. https://doi.org/10.1016/j.mtcomm.2023.106582
[42] W.M. Tucho, P. Cuvillier, A. Sjolyst-Kverneland, V. Hansen: Materials Science and Engineering: A, 689, 2017, 220-232. https://doi.org/10.1016/j.msea.2017.02.062
[43] J. Bae, Y. Kim, J.G. Kim, S. Kim, Journal of Materials Research and Technology, 33, 2024, 5384-5396. https://doi.org/10.1016/j.jmrt.2024.10.194